PEDOT counterions enabled oriented polyaniline nanorods for high performance flexible supercapacitors

Colloids and Surfaces A: Physicochemical and Engineering Aspects

Jin, Yingzhi; Li, Zongyu; Huang, Sanqing; Ning, Weihua; Yang, Xiaoming et al

https://doi.org/10.1016/j.colsurfa.2024.134461

Colloids and Surfaces A: Physicochemical and Engineering Aspects 697 (2024) 134461

Contents lists available at ScienceDirect

Colloids and Surfaces A: Physicochemical and Engineering Aspects

journal homepage: www.elsevier.com/locate/colsurfa

PEDOT counterions enabled oriented polyaniline nanorods for high performance flexible supercapacitors

Yingzhi Jin [a,*], Zongyu Li [a], Sanqing Huang [b,*], Weihua Ning [c], Xiaoming Yang [d], Yanfeng Liu [e], Zhen Su [a], Jiaxing Song [a], Lin Hu [a], XinXing Yin [a], Hao Lu [e], Han Zuilhof [a,f], Hao Wang [a], Zaifang Li [a,*]

[a] China-Australia Institute for Advanced Materials and Manufacturing, Jiaxing University, Jiaxing 314001, PR China
[b] National Engineering Lab of Textile Fiber Materials & Processing Technology (Zhejiang), Zhejiang Sci-Tech University, Hangzhou 310018, PR China
[c] Jiangsu Key Laboratory for Carbon-Based Functional Materials & Devices, Institute of Functional Nano & Soft Materials (FUNSOM), Soochow University, Suzhou 215123, PR China
[d] Zhejiang Fulai New Materials Co., Ltd, Jiaxing, 314117, PR China
[e] College of Materials and Textile Engineering, Nanotechnology Research Institute, Jiaxing University, Jiaxing 314001, PR China
[f] Laboratory of Organic Chemistry, Wageningen University and Research, Stippeneng 4, Wageningen 6708WE, the Netherlands

GRAPHICAL ABSTRACT

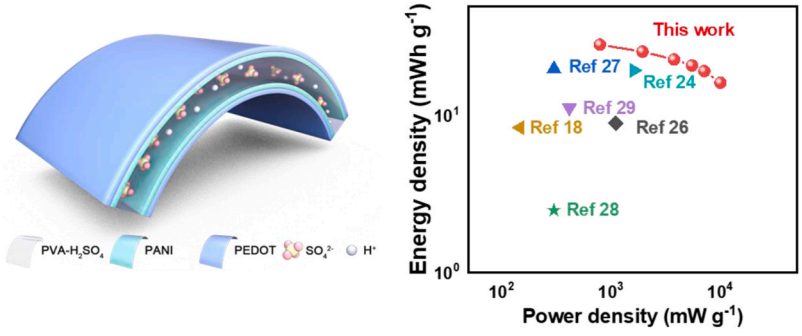

ARTICLE INFO

Keywords:
PANI
PEDOT counterion
Flexible supercapacitor
Nanorod structure

ABSTRACT

It is of great significance to prepare supercapacitors with high energy density and high stability for their application. In this work, we demonstrate that PEDOT/PANI:$(HSO_4^-)_X$:$(CF_3SO_3^-)_{1-X}$ composite electrodes obtained by in-situ polymerization and electrochemical polymerization with oriented nanorods structure can facilely assemble into flexible supercapacitors. An outstanding specific capacitance of 1042.7 F g^{-1} is achieved for PEDOT/PANI:$(HSO_4^-)_X$:$(CF_3SO_3^-)_{1-X}$ composite electrode under the condition of 10 mV s^{-1} in 1 M H_2SO_4 electrolyte. It is found that PANI grown on PEDOT has a rod-like structure with interpenetrating networks, which provides a high specific surface area and increased electron transmission channels. As a result, the specific capacitance of the assembled flexible supercapacitor reaches 361.6 F g^{-1}, with 71 % capacitance retention after 10,000 cycles. The flexible supercapacitor delivers a high energy density of 28.5 mWh g^{-1} at a power density of

* Corresponding authors.
E-mail addresses: yingzhi.jin@zjxu.edu.cn (Y. Jin), huangsq@zstu.edu.cn (S. Huang), zaifang.li@zjxu.edu.cn (Z. Li).

https://doi.org/10.1016/j.colsurfa.2024.134461
Received 22 March 2024; Received in revised form 21 May 2024; Accepted 3 June 2024
Available online 4 June 2024

789.5 mW g^{-1}. This work shows that PEDOT/PANI:$(HSO_4^-)_X$:$(CF_3SO_3^-)_{1-X}$ composite electrode is a promising electrode material for flexible supercapacitors.

1. Introduction

Supercapacitors with the advantages of rapid charge-discharge rate, high power density, and prolonged cyclic stability, are receiving more and more attention [1]. Carbon-based materials [2], metal oxides [3], and conducting polymers [4] are intensively investigated as active materials for supercapacitors. Carbon-based materials with good cycle stability but exhibit poor specific capacitance [5]. Metal oxides with superior Faradic redox capacity show better energy density. However, the commercial viability of RuO_2 is constrained by its high cost, while the low conductivity of MnO_2 also impedes its widespread adoption [6]. Conductive polymers (polypyrrole (PPy) [7], polyacetylene, polyaniline (PANI) [8], and poly(3,4-ethylenedioxythiophene) (PEDOT) [9]) are promising materials for the manufacturing of flexible supercapacitors due to their high conductivity, high pseudo-capacitance, good mechanical flexibility, and low-cost [10].

PANI is one of the most attractive conducting polymers in view of its high theoretical specific capacitance (2000 F g^{-1}) and unique proton doping mechanism [11]. However, at the start of this study, the actual capacitance of PANI electrodes was still lagging far behind the theoretical value [12]. Wang et al. constructed hyper-conjugated PANI with long conjugate chains. A specific capacitance of 512 F g^{-1} is obtained with 89.7 % capacitance retention after 10,000 cycles [8]. Somasundaram et al. prepared the manganese ferrite ($MnFe_2O_4$) grafted polyaniline nanocomposite electrode. A capacitance of 287.1 F g^{-1} was achieved with a rate capability of 57.3 % from 1 to 7 A g^{-1} [13]. In addition, the low energy density and poor cycle stability have limited the realization of any practical application as flexible supercapacitors. This dichotomy between high potential but limited realization has recently motivated many researchers to work on PANI electrodes to tackle these problems. PEDOT is widely used as an electrode material with excellent conductivity and good cycle stability. Nie et al. reported a novel PEDOT complex with a specific capacitance of 194 F cm^{-3} and a capacitance retention rate of 98 % after 10,000 cycles [14]. PEDOT is often used with PANI to form composite electrodes with new structures and high performance [15]. This has been used by many recent groups to develop improved materials. For example, Shahbaz et al. electrochemically polymerized PANI, PEDOT, and active carbon together to obtain a composite electrode. The capacitance of the electrode can reach 611 F g^{-1} at a current density of 1 A g^{-1} [16]. Liu et al. used a technique of one-dimensional self-assembly to prepare PEDOT: poly (styrene sulfonic acid)/PANI (PEDOT:PSS/PANI) fibers. The composite electrode has a specific capacitance of 367.7 F g^{-1} at a current density of 0.5 A g^{-1} [17]. Yang et al. integrated PANI and PEDOT through a molecular bridge provided by phytic acid. The assembled supercapacitor shows high volumetric energy density of 0.25 mWh cm^{-3} at a power density of 107.14 mW cm^{-3} [18]. Hierarchical porous RGO/PEDOT/PANI hybrid electrode was obtained through complex preparation process including two acid treatment by Liu et al.[19]. A high capacitance of 535 F g^{-1} along with a rate capability of 72.6 % in the current density ranging from 1 A g^{-1}~15 A g^{-1} was obtained. The electrode achieves a high energy density of 26.89 Wh kg^{-1} at a power density of 800 W kg^{-1}. While the progress was substantial, achieving high capacitance, high rate capability, and high cycle stability simultaneously is still an urgent problem for PANI-based supercapacitors.

One way to potentially improve the performance of PANI is by imposing order on the polymer structures. Chen et al. reported an ionic crosslink method to improve the order of PANI chains, exhibiting a specific capacitance of 419 F g^{-1}, which was four times higher than the control sample without the ionic crosslinker [20]. Sha et al. grew ordered nano-rod PANI on polystyrene nanospheres by chemical oxidative polymerization, resulting in a specific capacitance of 753 F g^{-1} at the current density of 1 A g^{-1}. This material was successfully embedded in a device, and after 1000 cycles, the retention rate of the capacitance was still 85.5 % [21]. These studies indicated that obtaining molecular order is indeed an effective means to improve the electrochemical performance of PANI.

The current paper focuses on the combination of a precisely defined electrochemical polymerization, and highly conductive PEDOT as a substrate to obtain an ordered PEDOT/PANI:$(HSO_4^-)_X$:$(CF_3SO_3^-)_{1-X}$ electrode, with a significant fraction of $CF_3SO_3^-$ as counterion in the PEDOT. We hypothesized that this superacid-derived anion might yield a higher degree of protonation onto the PANI polymer, and as such lead to more interchain interactions and concomitant molecular order. A high specific capacitance of 1042.7 F g^{-1} is achieved for the PEDOT/PANI:$(HSO_4^-)_X$:$(CF_3SO_3^-)_{1-X}$ electrode, which is 48.9 % higher than that of PANI:HSO_4^-. This material was then used for systematic studies of its potential as the electrode material for all-solid supercapacitors. Moreover, the assembled flexible supercapacitor based on PEDOT/PANI:$(HSO_4^-)_X$:$(CF_3SO_3^-)_{1-X}$ electrode shows a maximum energy density of 28.5 mWh g^{-1} at the power density of 789.8 mW g^{-1}, and a considerable cycle stability with 71 % of its initial capacitance after 10,000 charge/discharge cycles. This paper outlines these studies in detail and provides suggestions to even further improve this high-potential material for use in the 21st century energy transition.

2. Experimental

2.1. Materials

3,4-Ethylenedioxhythiophene (EDOT), sulphuric acid, iron (III) trifluoromethanesulfonate ($Fe(OTf)_3$), ethanol, aniline, polyethylene glycol-polypropylene glycol-polyethylene glycol (PEG-PPG-PEG; Mn=5800 Da) were all purchased from Anhui Senrise Technology Co., Ltd, and used without further purification. Deionized water obtained from DROIDE Ultra-pure water instrument (ZD-DI-Micro-30) was used for all aqueous solutions.

2.2. Preparation of the PEDOT film

PEDOT films with high conductivity were obtained by in-situ oxidative polymerization (O-polymerization) of EDOT on an ITO glass substrate. First, PEG-PPG-PEG (2 g, 0.17 mmol) as the polymerization rate controller was mixed with ethanol (10 mL) (1:4 mass ratio of polymer:ethanol) and shaken evenly. Then, 126 mg of oxidant $Fe(OTf)_3$ was added into 1 mL of the mixed solution under ambient atmosphere. After ultrasonic treatment for 3 h, 20 μL of EDOT monomer was added. Finally, the solution was spin-coated on an ITO glass or PET substrate at 3000 rpm for 40 s, followed by thermal annealing at 100 °C for 10 min.

2.3. Preparation of PEDOT/PANI:$(HSO_4^-)_X$:$(CF_3SO_3^-)_{1-X}$ composite film

PEDOT/PANI:$(HSO_4^-)_X$:$(CF_3SO_3^-)_{1-X}$ thin films were obtained by electrochemical polymerization (E-polymerization) of aniline onto a PEDOT substrate for 900 s at a constant current density of 1 mA cm^{-2}. In the three-electrode system, 0.05 M aniline was added into 0.5 M H_2SO_4 electrolytes, where Ag/AgCl was used as the reference electrode, a platinum electrode was used as the counter electrode, and the PEDOT thin film was used as the working electrode. The thickness of PEDOT and PANI is about 69 nm and 199 nm, the density of PEDOT and PANI is calculated to be 1 mg cm^{-3} and 1.1 mg cm^{-3}, and the area of the electrode is 0.75 cm^2, which giving the mass of PEDOT/PANI:$(HSO_4^-)_X$:

$(CF_3SO_3^-)_{1-X}$ electrode to be approximately 2.16×10^{-5} g. The mass ratio of PEDOT and PANI is approximately 1:3.15. To study the effect of the PEDOT substrate, under the same conditions, an ITO substrate was used as the working electrode to obtain a PANI:HSO_4^- film. This was used as the control system (*vide infra*). The thickness of PANI:HSO_4^- film is 130 nm, thus the mass of the PANI:HSO_4^- electrode is approximately 1.07×10^{-5} g.

2.4. Fabrication of all-solid supercapacitors

The all-solid supercapacitors were fabricated by bar coating a H_2SO_4-polyvinyl alcohol (PVA) hydrogel electrolyte on the top of PEDOT/PANI:$(HSO_4^-)_X$:$(CF_3SO_3^-)_{1-X}$ electrodes, and allowing these electrodes to dry under ambient conditions for 4 h. Then two of such electrodes with H_2SO_4-PVA electrolyte were gently pressed together and kept for 20 min to obtain a flexible supercapacitor. The H_2SO_4-PVA hydrogel was prepared by dissolving 1 g PVA power in 10 mL deionized water. The mixture was heated to 85 °C under stirring for 3 h. Then 1 g concentrated H_2SO_4 (98 %) was slowly added into the cooling down dispersion to produce the hydrogel.

2.5. Electrochemical measurements

An electrochemical workstation (model CHI660E, CH Instruments) was used for all electrochemical measurements. The electrochemical performance of PANI:HSO_4^- and PEDOT/PANI:$(HSO_4^-)_X$:$(CF_3SO_3^-)_{1-X}$ electrodes were investigated in a three-electrode system with 1 M H_2SO_4 as the electrolyte, platinum as the counter electrode and standard Ag/AgCl as the reference electrode. The galvanostatic charge and discharge (GCD) profile, cyclic voltammetry (CV) curve, and electrochemical impedance spectroscopy (EIS) of the electrode were measured in 1 M H_2SO_4 solution. The specific capacitance of electrodes in the three-electrode system was calculated from the CV curve according to the following equation:

$$C = \frac{1}{s\Delta V}\int j dV \tag{1}$$

wherein C is the specific capacitance (F g^{-1}), s is the scan rate (V/s), ΔV is the voltage window (V), j is the current density (A g^{-1}).

The specific mass capacitance (F g^{-1}) of all solid-state supercapacitors was calculated from the GCD profile using the following equation:

$$C = \frac{I\Delta t}{\Delta V} \tag{2}$$

Where I is the discharge current density (A g^{-1}), Δt is the discharge time (s), ΔV is the voltage window (V) after the current drops. The mass of two electrodes was used to calculate the discharge current density.

The energy density (E, mWh g^{-1}) and power density (P, mW g^{-1}) of supercapacitors can be calculated by Eqs. (3) and (4), respectively:

$$E = \frac{C\times(\Delta V)^2}{2\times3.6} \tag{3}$$

$$P = \frac{E\times3600}{\Delta t} \tag{4}$$

2.6. Other measurements

The thicknesses of films were measured by a stylus profilometer (DektakXT, Bruker). Scanning electron microscopy (SEM, Hitachi Regulus 8100), X-ray photoelectron spectroscopy (XPS, Thermo K-Alpha), and Grazing Incidence X-ray Diffraction (GIXRD, Bruker D8) were used to characterize the surface morphology and composition of PANI:HSO_4^- and PEDOT/PANI:$(HSO_4^-)_X$:$(CF_3SO_3^-)_{1-X}$ electrodes.

3. Results and discussion

3.1. Preparation and characterization of electrodes

The procedure for preparing the PANI:HSO_4^- and PEDOT/PANI:$(HSO_4^-)_X$:$(CF_3SO_3^-)_{1-X}$ electrodes is schematically described in Fig. 1a. The PEDOT electrode with $CF_3SO_3^-$ as the counterion was first fabricated by *in situ* oxidative polymerization (O-polymerization) of EDOT on an ITO substrate. PEDOT/PANI:$(HSO_4^-)_X$:$(CF_3SO_3^-)_{1-X}$ electrodes were obtained by electrochemical polymerization (E-polymerization) of aniline on a PEDOT substrate (see Experimental Section for details). In parallel, PANI:HSO_4^- electrodes were also prepared by E-polymerization on ITO as the reference. As illustrated in Fig. 1b, PANI:HSO_4^- is polymerized with HSO_4^- as the sole counterion on ITO substrates. When the polymerization was achieved on PEDOT, this included the $CF_3SO_3^-$ anions already present in PEDOT, which thus formed part of the new complex of PANI:$(HSO_4^-)_X$:$(CF_3SO_3^-)_{1-X}$ on PEDOT substrate. The formation of the new complex is confirmed by the XPS results which will be discussed in detail in the following part.

The morphologies of the resulting PANI:HSO_4^- and PEDOT/PANI:$(HSO_4^-)_X$:$(CF_3SO_3^-)_{1-X}$ electrodes are revealed by SEM, as shown in Fig. 2. It can be seen from Fig. 2a that PANI: HSO_4^- forms a nanosphere structure on top of the ITO substrate, with an uneven distribution of both the size and location of these nanospheres. Such a thin layer of nanospheres does not yield a high specific surface area of the resulting electrodes. In contrast, PANI polymerized on PEDOT shows a nanorod structure, which can be clearly identified in Fig. 2b. Such a nanorod structure provides a significantly larger specific surface area for the Faraday reaction, and thus more ion transmission channels for the insertion and extraction of electrolyte ions. This finding hinted at the possibility of using PEDOT/PANI:$(HSO_4^-)_X$:$(CF_3SO_3^-)_{1-X}$ as electrodes in supercapacitor devices that hinge on such large specific surface areas.

XPS was used to investigate the surface element composition and the chemical state of these components, the results are displayed in Fig. 2c-f. The survey spectra in Fig. 2c manifest the S, C, N, and O elements for both PANI:HSO_4^- and PEDOT/PANI:$(HSO_4^-)_X$:$(CF_3SO_3^-)_{1-X}$ samples. It is worth noting that S2p and O1s on the PANI:HSO_4^- and PEDOT/PANI:$(HSO_4^-)_X$:$(CF_3SO_3^-)_{1-X}$ electrodes come from the counterion of HSO_4^- and $CF_3SO_3^-$. In addition, compared with PANI:HSO_4^-, the existence of F1s in the XPS spectrum of PEDOT/PANI:$(HSO_4^-)_X$:$(CF_3SO_3^-)_{1-X}$ indicates that $CF_3SO_3^-$ from PEDOT bottom layer has been successfully doped into PANI. It can be seen from Fig. 2d that after PEDOT is soaked in sulfuric acid, the F1s peak in the survey XPS spectrum of PEDOT-sulf has disappeared, due to the substitution of $CF_3SO_3^-$ by HSO_4^-. Due to the higher acidity of CF_3SO_3H compared to H_2SO_4, PEDOT/PANI:$(HSO_4^-)_X$:$(CF_3SO_3^-)_{1-X}$ shows a higher degree of protonation than PANI:HSO_4^-. It is worth mentioning that the existence of F element in PEDOT/PANI:$(HSO_4^-)_X$:$(CF_3SO_3^-)_{1-X}$ is also confirmed in the element mapping diagram in Fig. S1 (ESI). The dopant-to-polymer ratio could be calculated from the XPS spectra as the S/N atom ratio. The S/N atom ratio of PANI:HSO_4^- and PEDOT/PANI:$(HSO_4^-)_X$:$(CF_3SO_3^-)_{1-X}$ is 0.329 and 0.369, demonstrating a higher degree of oxidation in PEDOT/PANI:$(HSO_4^-)_X$:$(CF_3SO_3^-)_{1-X}$ electrode. Furthermore, the ratio of dopants HSO_4^-:$CF_3SO_3^-$ in the PEDOT/PANI:$(HSO_4^-)_X$:$(CF_3SO_3^-)_{1-X}$ electrode is 1:0.317. The total content of dopants is calculated from the area of S2p. The content of dopant $CF_3SO_3^-$ is calculated from the area of F1s divided by 3.

Fig. 2e and f show N1s XPS spectra of PEDOT/PANI:$(HSO_4^-)_X$:$(CF_3SO_3^-)_{1-X}$ and PANI:HSO_4^- electrodes, respectively. The N1s peak is further deconvoluted into three peaks at 399.2, 400.1, and 401.2 eV, corresponding to the quinoid imine (-N=), benzenoid amine (-NH-), and cationic nitrogen (-N^+-) in PEDOT/PANI:$(HSO_4^-)_X$:$(CF_3SO_3^-)_{1-X}$, respectively [22]. For PANI:HSO_4^-, these peaks move to lower binding energies at 398.9, 399.6, and 401.0 eV, respectively. Furthermore, the contents of quinoid imine and cationic nitrogen in PEDOT/PANI:$(HSO_4^-)_X$:$(CF_3SO_3^-)_{1-X}$ are more than those in PANI:HSO_4^-, indicating a high degree of protonation [23]. Such increased protonation provides the option for

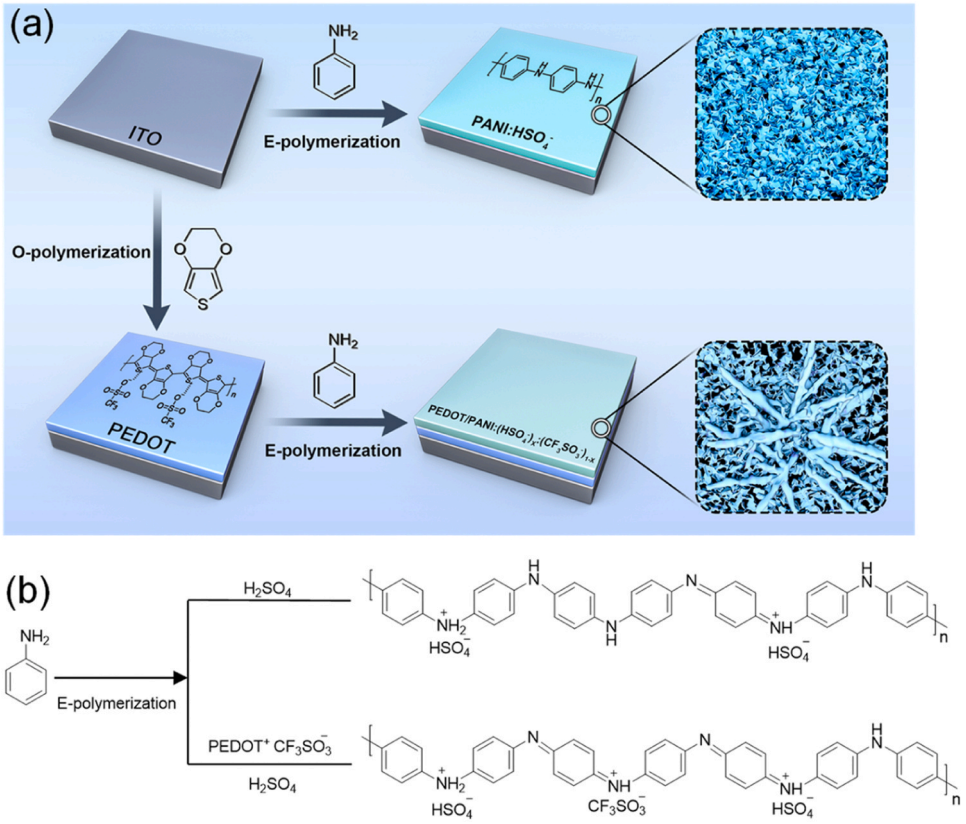

Fig. 1. (a) Schematic illustration of the preparation process of PANI:HSO_4^- and PEDOT/PANI:$(HSO_4^-)_X$:$(CF_3SO_3^-)_{1-X}$ electrodes. (b) Schematic illustration of the molecular structures of PANI:HSO_4^- and PANI:$(HSO_4^-)_X$:$(CF_3SO_3^-)_{1-X}$.

increased interchain hydrogen bridging, thus making the interaction between PANI main chains stronger and inducing ordering.

The XRD pattern of PANI:HSO_4^- and PEDOT/PANI:$(HSO_4^-)_X$:$(CF_3SO_3^-)_{1-X}$ are shown in Fig. S2 (ESI), where similar peaks at 21.4°, 30.4° and 35.4° are presented. It revealed that these peaks in PEDOT/PANI:$(HSO_4^-)_X$:$(CF_3SO_3^-)_{1-X}$ are stronger compared to that of PANI:HSO_4^-, indicating a higher crystallinity of the composite film, matching well with its nanorod structure on the SEM images.

3.2. Electrochemical performance of electrodes

The electrochemical performance of PANI:HSO_4^- and PEDOT/PANI:$(HSO_4^-)_X$:$(CF_3SO_3^-)_{1-X}$ were analyzed in a three-electrode system. The CV curves and GCD profile of the PANI:HSO_4^- and PEDOT/PANI:$(HSO_4^-)_X$:$(CF_3SO_3^-)_{1-X}$ electrodes are shown in Fig. 3. Both of them show a quasi-rectangular shape with three obvious redox peaks in the CV curves (Fig. 3a & b) at scan rates ranging from 10 to 200 mV s^{-1}, which indicate the coexistence of double layer capacitance and pseudocapacitance. The current response increases with the increase of the scan rates for both of the electrodes. These three pairs of redox peaks in the CV curve of PANI correspond to the redox transition between leucoemeraldine and protonated emeraldine, the redox transition between emeraldine and pernigraniline, and the redox transition between benzoquinone and hydroquinone [24]. In order to have a clearer view to see the rate capability, CV curves normalized to scan rate are shown in Fig. S3 in ESI. Both of the electrodes display a good quasi-rectangular shape up to 200 mV s^{-1}, which indicates a good rate capability. The non-linear characteristics of the GCD curves (Fig. 3c & d) further confirm the redox behavior of PANI.

Compared with PANI:HSO_4^-, the CV curve of PEDOT/PANI:$(HSO_4^-)_X$:$(CF_3SO_3^-)_{1-X}$ encloses a larger area at the scan rate of 10 mV s^{-1} (Fig. 4a), *i.e.* PEDOT/PANI:$(HSO_4^-)_X$:$(CF_3SO_3^-)_{1-X}$ has a higher specific capacitance. At the same time, this conclusion is proved by comparing the discharge time of PANI:HSO_4^- and PEDOT/PANI:$(HSO_4^-)_X$:$(CF_3SO_3^-)_{1-X}$ electrodes at the same charge density, which are shown in Figs. 3c and 3d. In addition, the leakage current (Fig. S4a in ESI) declined significantly from 0.2 mA to 6.2 μA after 10 min for PANI:HSO_4^- electrode, the leakage current declined from 0.5 mA to 15.1 μA after 10 min for PEDOT/PANI:$(HSO_4^-)_X$:$(CF_3SO_3^-)_{1-X}$ electrode. The small leakage current could be ascribed to the self-discharge process of the electrode material. The PEDOT/PANI:$(HSO_4^-)_X$:$(CF_3SO_3^-)_{1-X}$ electrode shows a better self-discharge property, the voltage is above 0.4 V after 6 h (Fig. S4b in ESI), while the voltage of PANI:HSO_4^- electrode only managed to remain 0.3 V after 6 h. In comparison with previously reported PANI-based electrodes, the voltage is dropped to one-half of the initial value within 13 min for PEDOT/PANI hydrogel [18].

The specific capacitance of PEDOT/PANI:$(HSO_4^-)_X$:$(CF_3SO_3^-)_{1-X}$ and PANI:HSO_4^- electrodes are calculated from the CV and GCD curves shown in Fig. 4b and c. From the CV curves, the PEDOT/PANI:$(HSO_4^-)_X$:$(CF_3SO_3^-)_{1-X}$ electrode delivered a champion specific capacitance of 1042.7 F g^{-1} (1120.5 F cm^{-3}) at the scan rate of 10 mV s^{-1}, which is higher than that of PANI:HSO_4^- (700.5 F g^{-1}, 770.6 F cm^{-3}). The specific capacitances from GCD profiles are 995.3 F g^{-1} and 672.4 F g^{-1} for PEDOT/PANI:$(HSO_4^-)_X$:$(CF_3SO_3^-)_{1-X}$ and PANI:HSO_4^- electrodes at 2.5 A g^{-1}, respectively. PEDOT/PANI:$(HSO_4^-)_X$:$(CF_3SO_3^-)_{1-X}$ electrode remains its 76.1 % initial capacitance at 30 A g^{-1}, PANI:HSO_4^- electrode remains its 77.9 % initial capacitance at 30 A g^{-1}. The coulombic efficiencies of PEDOT/PANI:$(HSO_4^-)_X$:$(CF_3SO_3^-)_{1-X}$ and PANI:HSO_4^- electrodes are calculated from the GCD profiles shown in Fig. 4d. The coulombic efficiency of PEDOT/PANI:$(HSO_4^-)_X$:$(CF_3SO_3^-)_{1-X}$ under the current density of 2.5 A g^{-1} is 86.1 %, slightly higher than that of PANI:HSO_4^- (85.2 %), and both electrodes exhibit even higher coulombic efficiencies (above 90 %) under high current densities. The cyclic stability of PEDOT/PANI:$(HSO_4^-)_X$:$(CF_3SO_3^-)_{1-X}$ and PANI:HSO_4^- electrodes are

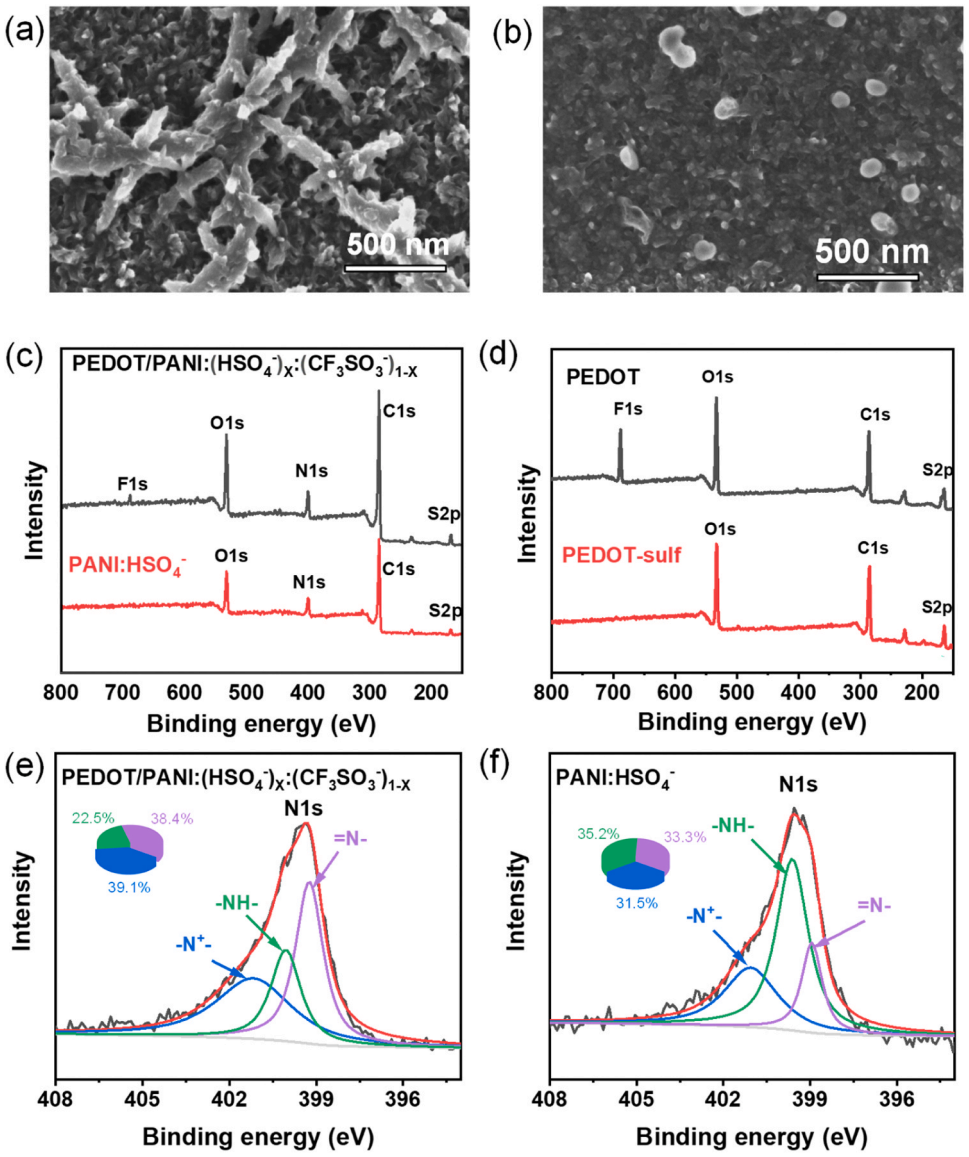

Fig. 2. SEM images of PANI:HSO_4^- (a) and PEDOT/PANI:$(HSO_4^-)_X$:$(CF_3SO_3^-)_{1-X}$ (b). (c) XPS survey spectra of PEDOT/PANI:$(HSO_4^-)_X$:$(CF_3SO_3^-)_{1-X}$ and PANI:HSO_4^-. (d) XPS survey spectra of PEDOT and PEDOT-sulf (with H_2SO_4 treatment). (e) N1s spectrum of PEDOT/PANI:$(HSO_4^-)_X$:$(CF_3SO_3^-)_{1-X}$. (f) N1s spectrum of PANI:HSO_4^-.

shown in Fig. S5. PEDOT/PANI:$(HSO_4^-)_X$:$(CF_3SO_3^-)_{1-X}$ electrode displays a capacitance retention rate of 85.4 % after 10,000 cycles at a current density of 30 A g^{-1}. PANI:HSO_4^- electrode is only 71 %. PEDOT/PANI:$(HSO_4^-)_X$:$(CF_3SO_3^-)_{1-X}$ electrode has better coulombic efficiency and cyclic stability than PANI:HSO_4^- electrode, but it still needs to be improved compared with inorganic materials to achieve practical applications. This capacitance result of the PANI:HSO_4^- and PEDOT/PANI:$(HSO_4^-)_X$:$(CF_3SO_3^-)_{1-X}$ electrodes is compared to a range of previously reported PANI-based materials and inorganic materials in Table 1. The capacitance of PEDOT/PANI:$(HSO_4^-)_X$:$(CF_3SO_3^-)_{1-X}$ electrode surpasses that of previous reported PANI-based electrodes. When comparing with inorganic materials such as RuO_2, PEDOT/PANI:$(HSO_4^-)_X$:$(CF_3SO_3^-)_{1-X}$ electrode has the advantages of low-cost and flexibility, despite having a slightly smaller specific capacitance. We attribute this higher specific capacitance of the PEDOT/PANI:$(HSO_4^-)_X$:$(CF_3SO_3^-)_{1-X}$ electrode to three factors: 1) A PEDOT substrate with $CF_3SO_3^-$ counterions can likely more easily adsorb homogeneous protonated aniline to induce the polymerization. 2) The doping of $CF_3SO_3^-$ in PANI leads to a higher protonation degree and higher conductivity. 3) The nanorod structure leads to a higher available surface area, thus providing more active sites for the Faraday reaction, and thereby more ion transmission channels for the insertion and extraction of electrolyte ions.

3.3. Electrochemical performance of all-solid supercapacitors

In order to evaluate the practical feasibility of this composite materials, two PEDOT/PANI:$(HSO_4^-)_X$:$(CF_3SO_3^-)_{1-X}$ electrodes are attached by PVA-H_2SO_4 gel to form a flexible all-solid supercapacitor, as illustrated in Fig. 5a. The electrochemical performance was tested in a two-electrode system. The CV curves of the flexible supercapacitor based on PEDOT/PANI:$(HSO_4^-)_X$:$(CF_3SO_3^-)_{1-X}$ electrode are shown in Fig. 5b. It can be seen that although there are redox peaks in its CV curve, it is far less obvious than those in the CV data of the electrode in H_2SO_4 electrolyte (Fig. 4a), which may be due to the relatively slow ion transport in PVA-H_2SO_4 gel electrolyte. Based on the CV curves, the specific capacitance of the flexible supercapacitor is 361.6 F g^{-1} at the scan rate of 10 mV s^{-1} (Fig. S6 in ESI). This value is 34.7 % of the PEDOT/PANI:$(HSO_4^-)_X$:$(CF_3SO_3^-)_{1-X}$ electrode in H_2SO_4 electrolyte. According to the GCD profiles in Fig. 5c, the specific capacitance of the flexible supercapacitor is 329 F g^{-1} at the current density of 2 A g^{-1} and remains at

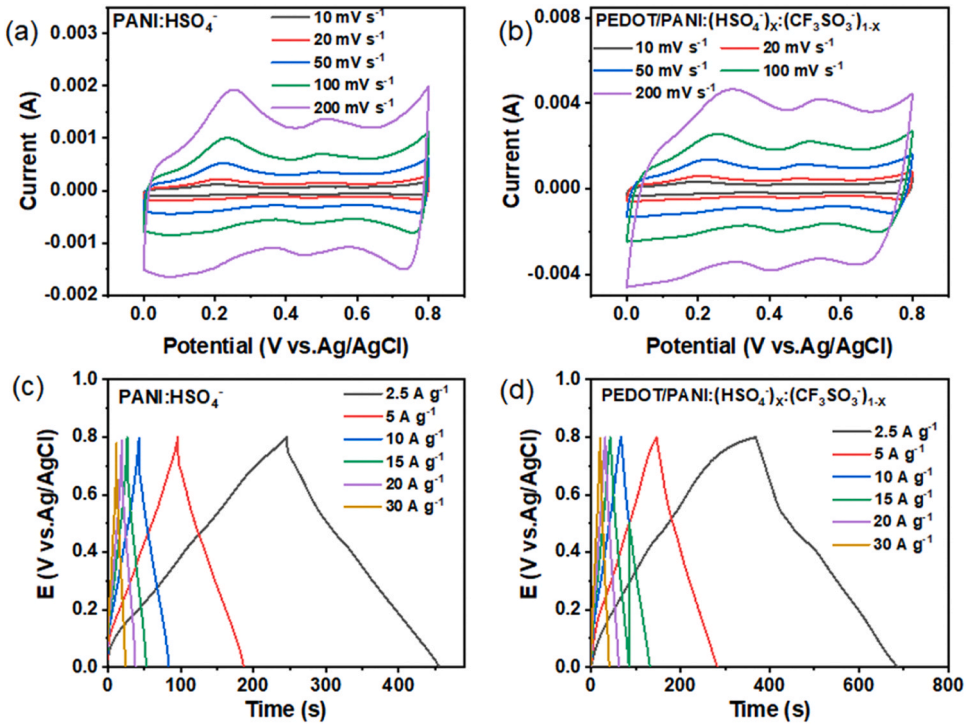

Fig. 3. CV curves of (a) PANI:HSO_4^- and (b) PEDOT/PANI:$(HSO_4^-)_X$:$(CF_3SO_3^-)_{1-X}$ under different scan rates. GCD curves of PANI:HSO_4^- (c) and PEDOT/PANI:$(HSO_4^-)_X$:$(CF_3SO_3^-)_{1-X}$ (d) at different current densities. The thickness of PANI:HSO_4^- film is 130 nm (mass: 1.07×10^{-5} g), the thickness of PEDOT/PANI:$(HSO_4^-)_X$:$(CF_3SO_3^-)_{1-X}$ is 268 nm (69 nm PEDOT and 199 nm PANI, mass: 2.16×10^{-5} g).

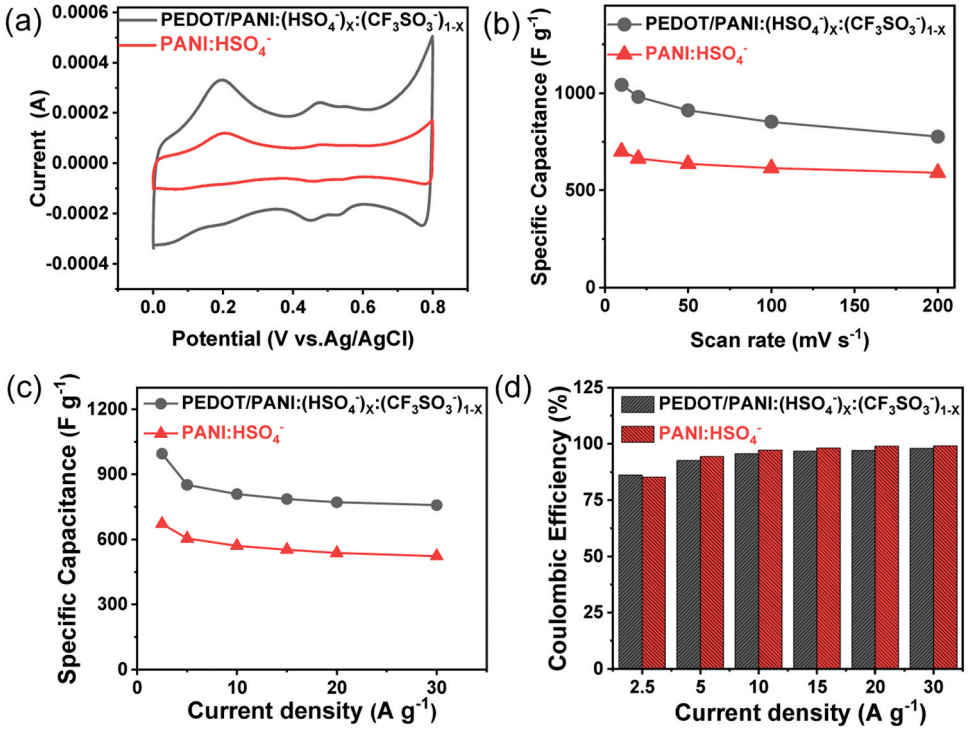

Fig. 4. (a) CV curves of PANI:HSO_4^- and PEDOT/PANI:$(HSO_4^-)_X$:$(CF_3SO_3^-)_{1-X}$ under scan rates of 10 mV s^{-1}. (b) Specific capacitance of PEDOT/PANI:$(HSO_4^-)_X$:$(CF_3SO_3^-)_{1-X}$ and PANI:HSO_4^- at different scan rates. The thickness of PANI:HSO_4^- film is 130 nm (mass: 1.07×10^{-5} g), the thickness of PEDOT/PANI:$(HSO_4^-)_X$:$(CF_3SO_3^-)_{1-X}$ is 268 nm (69 nm PEDOT and 199 nm PANI, mass: 2.16×10^{-5} g). (c) Specific capacitance of PEDOT/PANI:$(HSO_4^-)_X$:$(CF_3SO_3^-)_{1-X}$ and PANI:HSO_4^- at different current densities. (d) Coulombic efficiencies of PEDOT/PANI:$(HSO_4^-)_X$:$(CF_3SO_3^-)_{1-X}$ and PANI:HSO_4^- at different current densities.

80.9 % of the initial capacitance at the current density of 30 A g^{-1} (Fig. 5d), which indicates high rate capability of the flexible devices. The cycle stability of the flexible supercapacitor is analyzed by GCD measurements at 30 A g^{-1}. After 10,000 charge and discharge cycles, 71 % of the original specific capacitance could be maintained with coulombic efficiencies higher than 90 % (Fig. 5e), suggesting excellent

Table 1
Comparison of the specific capacitance of current work with previously reported PANI-based materials and inorganic materials.

Material	Specific capacitance	Potential interval	Ref.
PANI-B	419 F g^{-1}	-0.2–0.8 V[a]	[20]
DMSO-PEDOT:PSS/PANi	367.7 F g^{-1}	-0.2–0.8 V[a]	[17]
rGO/PANI-3	871.5 F g^{-1}	-0.2–0.8 V[a]	[22]
PANI@PC	346 F g^{-1}	0.4–1.4 V[b]	[12]
hc-PANI	521 F g^{-1}	0–0.7 V[c]	[8]
$Ti_3C_2T_x$ @PANI-RGO	617.84 F g^{-1}	-1–0 V[d]	[25]
PANI/MoOx@ $Ti_3C_2T_x$	450 F g^{-1}	-0.6–0 V[a]	[26]
$Ti_3C_2T_x$	245 F g^{-1}	-0.35–0.2 V[a]	[27]
$RuO_2{\cdot}xH_2O$	1300 F g^{-1}	0–1 V[a]	[28]
PANI:HSO_4^-	700.5 F g^{-1}	0–0.8 V[a]	This work
PEDOT/PANI:$(HSO_4^-)_X$:$(CF_3SO_3^-)_{1-X}$	1042.7 F g^{-1}	0–0.8 V[a]	This work

[a] 1 M H_2SO_4 aqueous solution, Ag/AgCl as reference electrode.
[b] 6 M KOH aqueous solution, Zn/ZnO as reference electrode.
[c] 1 M H_2SO_4 aqueous solution, saturated calomel as reference electrode.
[d] 1 M KOH, Ag/AgCl, Ag/AgCl as reference electrode.

performance in the PVA-H_2SO_4 gel electrolyte. The good capacitance performance and cycle stability can be attributed to the higher degree of oxidation, which is caused by $CF_3SO_3^-$ doping, and the improved surface morphology of the electrode. The Ragone plot (energy density (E_{Ca}) vs. power density (P_{Ca})) of the flexible supercapacitor is shown in Fig. 5f. The energy density of the flexible supercapacitor can reach up to 28.5 mWh g^{-1} at the power density of 789.8 mW g^{-1}, and retains an energy density of 16.3 mWh g^{-1} at the power density of 9945.8 mW g^{-1}. This outperforms previously reported supercapacitors based on PANI electrodes [20,26,29–32].

4. Conclusions

In summary, a high specific capacitance of 1042.7 F g^{-1} is demonstrated for the PEDOT/PANI:$(HSO_4^-)_X$:$(CF_3SO_3^-)_{1-X}$ composite electrode. This is attributed to the positive effects of $CF_3SO_3^-$ doping, increased ordering of the PANI polymer chains, and a higher specific surface area that results from an interpenetrating structure with oriented PANI nanorods on the PEDOT substrate. The resulting flexible supercapacitor delivered an outstanding energy density of 28.5 mWh g^{-1} at the power density of 789.8 mW g^{-1}, and even a high energy density of 16.3 mWh g^{-1} at the power density of 9945.8 mW g^{-1}. These results show that the PEDOT/PANI:$(HSO_4^-)_X$:$(CF_3SO_3^-)_{1-X}$ composite is an excellent electrode material for supercapacitors, provide new options for the practical application of supercapacitors in the future, and hopefully stimulates more work on ordered polymers in this field.

CRediT authorship contribution statement

Zhen Su: Investigation. **Jiaxing Song:** Methodology. **Lin Hu:** Software. **XinXing Yin:** Investigation. **Hao Lu:** Writing – review & editing. **Han Zuilhof:** Writing – review & editing, Software. **Yingzhi Jin:** Writing – review & editing, Supervision, Conceptualization. **Hao Wang:** Resources. **Zongyu Li:** Writing – original draft, Data curation. **Zaifang Li:** Supervision, Project administration, Funding acquisition. **Sanqing Huang:** Supervision, Project administration. **Weihua Ning:** Resources. **Xiaoming Yang:** Resources. **Yanfeng Liu:** Writing – review & editing.

Declaration of Competing Interest

The authors declare that they have no known competing financial interests or personal relationships that could have appeared to influence the work reported in this paper.

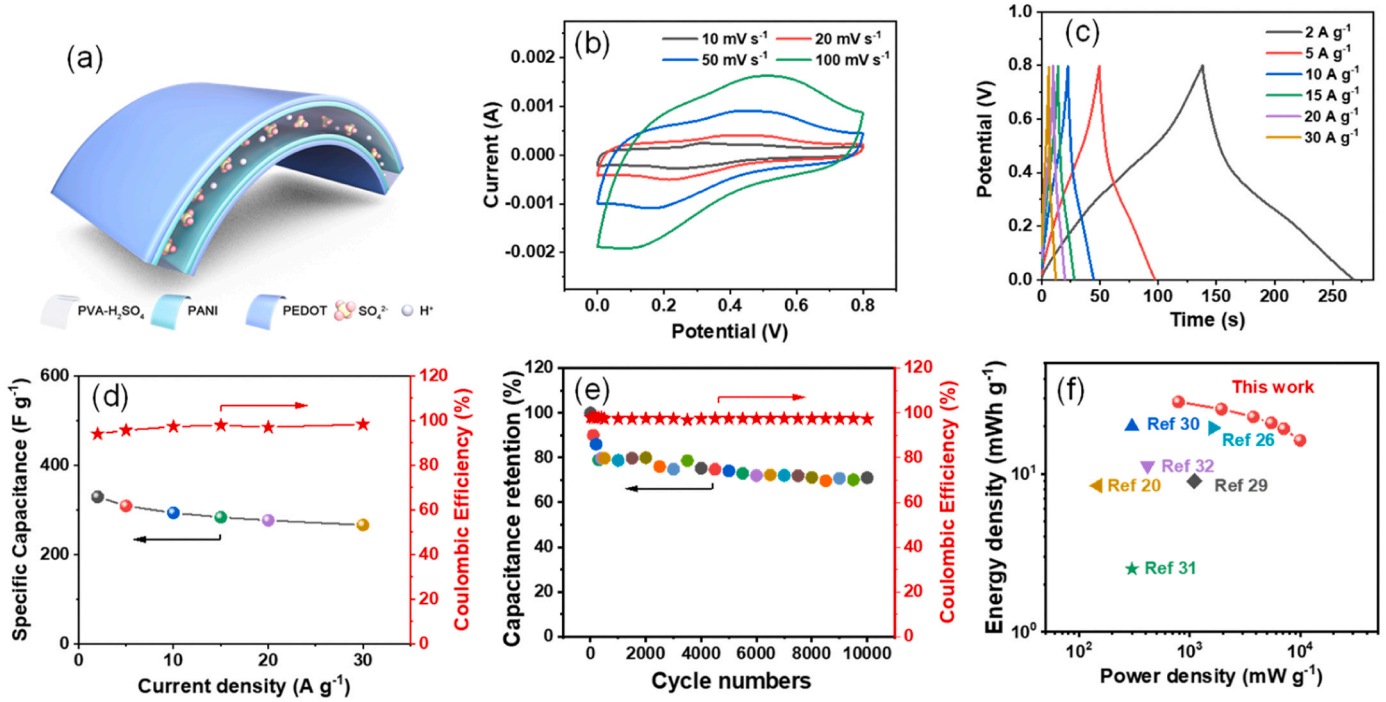

Fig. 5. (a) Schematic diagram of the flexible supercapacitor based on PEDOT/PANI:$(HSO_4^-)_X$:$(CF_3SO_3^-)_{1-X}$ electrodes. (b) CV curves of the flexible supercapacitor at different scan rates from 10 to 100 mV s^{-1}. (c) GCD profiles of the flexible supercapacitor at current densities from 2 to 30 A g^{-1}. (d) The specific capacitance and coulombic efficiency of the flexible supercapacitor calculated from the GCD profiles. (e) Capacitance retention and coulombic efficiency of the flexible supercapacitor at the current density of 30 A g^{-1}. (f) Ragone plot of the flexible supercapacitor compared with the previously reported supercapacitor based on PANI. The thickness of PEDOT/PANI:$(HSO_4^-)_X$:$(CF_3SO_3^-)_{1-X}$ is 268 nm (69 nm PEDOT and 199 nm PANI, mass: 2.16×10^{-5} g).

Data availability

No data was used for the research described in the article.

Acknowledgments

This work was supported by the Zhejiang Public Welfare Technology Application Research Program (LGJ22B040001), the Innovation Jiaxing·Elite Leading Plan 2020, the Jiaxing Science and Technology Project (2023AY40001), Fundamental Research Funds for the Jiaxing University (No. CD70520065), Scientific Research Fund of Zhejiang Provincial Education Department (Y202249407).

Appendix A. Supporting information

Supplementary data associated with this article can be found in the online version at doi:10.1016/j.colsurfa.2024.134461.

References

[1] L.N. Khandare, D.J. Late, N.B. Chaure, Molybdenum sulfoselenide nanocomposite material with PANI coating for supercapacitor applications, Surf. Interfaces 43 (2023) 103533, https://doi.org/10.1016/j.surfin.2023.103533.
[2] P. Wang, X. Zhang, W. Duan, W. Teng, Y. Liu, Q. Xie, Superhydrophobic flexible supercapacitors formed by integrating hydrogel with functional carbon nanomaterials, Chin. J. Chem. 39 (2021) 1153–1158, https://doi.org/10.1002/cjoc.202000543.
[3] Z. Peng, S. Li, Y. Huang, J. Guo, L. Tan, Y. Chen, Sodium-intercalated manganese oxides for achieving ultra-stable and fast charge storage kinetics in wide-voltage aqueous supercapacitors, Adv. Funct. Mater. 32 (2022) 2206539, https://doi.org/10.1002/adfm.202206539.
[4] Z. Su, Y. Jin, Y. Xiao, H. Zheng, Z. Yang, H. Wang, Z. Li, Excellent rate capability supercapacitor based on a free-standing PEDOT:PSS film enabled by the hydrothermal method, Chem. Commun. 58 (2022) 5088–5091, https://doi.org/10.1039/D2CC00427E.
[5] X. Liu, J. Wang, G. Yang, In situ growth of the Ni3V2O8@PANI composite electrode for flexible and transparent symmetric supercapacitors, ACS Appl. Mater. Interfaces 10 (2018) 20688–20695, https://doi.org/10.1021/acsami.8b04609.
[6] P. Simon, Y. Gogotsi, Perspectives for electrochemical capacitors and related devices, Nat. Mater. 19 (2020) 1151–1163, https://doi.org/10.1038/s41563-020-0747-z.
[7] Z. Sun, S. Eyley, Y. Guo, R. Salminen, W. Thielemans, Synergistic effects of chloride anions and carboxylated cellulose nanocrystals on the assembly of thick three-dimensional high-performance polypyrrole-based electrodes, J. Energy Chem. 70 (2022) 492–501, https://doi.org/10.1016/j.jechem.2022.03.004.
[8] Y. Wang, X. Chu, H. Zhang, C. Yan, G. Tian, W. Yang, X. Chen, H. Zhang, Hyper-conjugated polyaniline delivering extraordinary electrical and electrochemical properties in supercapacitors, Appl. Surf. Sci. 628 (2023) 157350, https://doi.org/10.1016/j.apsusc.2023.157350.
[9] R. Ravit, J. Abdullah, I. Ahmad, Y. Sulaiman, Electrochemical performance of poly (3, 4-ethylenedioxythipohene)/nanocrystalline cellulose (PEDOT/NCC) film for supercapacitor, Carbohydr. Polym. 203 (2019) 128–138, https://doi.org/10.1016/j.carbpol.2018.09.043.
[10] Q. Meng, K. Cai, Y. Chen, L. Chen, Research progress on conducting polymer based supercapacitor electrode materials, Nano Energy 36 (2017) 268–285, https://doi.org/10.1016/j.nanoen.2017.04.040.
[11] H. Li, J. Wang, Q. Chu, Z. Wang, F. Zhang, S. Wang, Theoretical and experimental specific capacitance of polyaniline in sulfuric acid, J. Power Sources 190 (2009) 578–586, https://doi.org/10.1016/j.jpowsour.2009.01.052.
[12] G. Jiang, J. Cai, M. Krishnamoorthy, R.A. Senthil, Y. Sun, X. Li, J. Pan, Controlling morphologies and structures of PANI@carbon with superior rate performance for supercapacitors, ACS Appl. Energy Mater. 5 (2022) 4138–4148, https://doi.org/10.1021/acsaem.1c03478.
[13] A.J. Somasundaram, H. Xiao, S. Pandiyarajan, A.-H. Liao, S. Lydia, H.-C. Chuang, In-situ fabrication of manganese ferrite grafted polyaniline nanocomposite: A magnetically reusable visible light photocatalyst and a robust electrode material for supercapacitor, J. Colloid Interface Sci. 642 (2023) 584–594, https://doi.org/10.1016/j.jcis.2023.03.170.
[14] S. Nie, Z. Li, Z. Su, Y. Jin, H. Song, H. Zheng, J. Song, L. Hu, X. Yin, Z. Xu, Y. Yao, H. Wang, Z. Li, Highly stable supercapacitors enabled by a new conducting polymer complex PEDOT:CF3SO2(x)PSS(1-x)**, ChemSusChem 16 (2023) e202202208, https://doi.org/10.1002/cssc.202202208.
[15] F.N. Ajjan, N. Casado, T. Rębiś, A. Elfwing, N. Solin, D. Mecerreyes, O. Inganäs, High performance PEDOT/lignin biopolymer composites for electrochemical supercapacitors, J. Mater. Chem. A 4 (2016) 1838–1847, https://doi.org/10.1039/C5TA10096H.
[16] S. Khan, M. Alkhedher, R. Raza, M.A. Ahmad, A. Majid, E.M.T.E. Din, Electrochemical investigation of PANI:PPy/AC and PANI:PEDOT/AC composites as electrode materials in supercapacitors, Polymers 14 (2022) 1976.
[17] G. Liu, X. Chen, C. Liu, Q. Jiang, F. Jiang, J. An, J. Xu, P. Liu, DMSO-treated flexible PEDOT:PSS/PANI fiber electrode for high performance supercapacitors, J. Mater. Sci. 56 (2021) 14632–14643, https://doi.org/10.1007/s10853-021-06226-0.
[18] Z. Yang, J. Ma, B. Bai, A. Qiu, D. Losic, D. Shi, M. Chen, Free-standing PEDOT/polyaniline conductive polymer hydrogel for flexible solid-state supercapacitors, Electrochim. Acta 322 (2019) 134769, https://doi.org/10.1016/j.electacta.2019.134769.
[19] F. Liu, L. Xie, L. Wang, W. Chen, W. Wei, X. Chen, S. Luo, L. Dong, Q. Dai, Y. Huang, L. Wang, Hierarchical porous rGO/PEDOT/PANI hybrid for planar/linear supercapacitor with outstanding flexibility and stability, Nano-Micro Lett. 12 (2020) 17, https://doi.org/10.1007/s40820-019-0342-5.
[20] X. Chen, P. Liu, C. Liu, G. Liu, J. Wei, J. Xu, Q. Jiang, X. Liu, F. Jiang, Microstructure control for high-capacitance polyaniline, Electrochim. Acta 391 (2021) 138977, https://doi.org/10.1016/j.electacta.2021.138977.
[21] S. Peng, B. Liu, X. Zhang, W. Li, S. Chen, C. Hu, X. Liu, J. Liu, J. Chen, Large-area polyaniline nanorod growth on a monolayer polystyrene nanosphere array as an electrode material for supercapacitors, ACS Appl. Energy Mater. 4 (2021) 14766–14777, https://doi.org/10.1021/acsaem.1c03524.
[22] Y. Yu, A. Xu, Y. Zhang, W. Li, Y. Qin, Evaporation-induced hydrated graphene/polyaniline/carbon cloth integration towards high mass loading supercapacitor electrodes, Chem. Eng. J. 445 (2022) 136727, https://doi.org/10.1016/j.cej.2022.136727.
[23] C. Zhou, S. He, H. Yang, J. An, L. Yang, P. Yan, H. Zhang, Influence of acidic type on nanostructures and electrochemical performance of polyaniline for flexible supercapacitors and improved performance based on 3D honeycomb-like nanosheet by doping hpf6 acid, Electrochim. Acta 390 (2021) 138818, https://doi.org/10.1016/j.electacta.2021.138818.
[24] A. Eftekhari, L. Li, Y. Yang, Polyaniline supercapacitors, J. Power Sources 347 (2017) 86–107, https://doi.org/10.1016/j.jpowsour.2017.02.054.
[25] P. Liao, Y. Zeng, Z. Qiu, S. Hao, J. He, H. Xu, S. Chen, 3D Ti3C2Tx@PANI-reduced graphene oxide hydrogel and defective reduced graphene oxide hydrogel as anode and cathode for high-energy asymmetric supercapacitor, J. Alloy. Compd. 948 (2023) 169593, https://doi.org/10.1016/j.jallcom.2023.169593.
[26] H. Xie, S. Ma, Z. He, Facile preparation of PANI/MoOx nanowires decorated MXene film electrodes for electrochemical supercapacitors, Electrochim. Acta 448 (2023) 142173, https://doi.org/10.1016/j.electacta.2023.142173.
[27] M. Ghidiu, M.R. Lukatskaya, M.-Q. Zhao, Y. Gogotsi, M.W. Barsoum, Conductive two-dimensional titanium carbide 'clay' with high volumetric capacitance, Nature 516 (2014) 78–81, https://doi.org/10.1038/nature13970.
[28] C.-C. Hu, K.-H. Chang, M.-C. Lin, Y.-T. Wu, Design and tailoring of the nanotubular arrayed architecture of hydrous RuO2 for next generation supercapacitors, Nano Lett. 6 (2006) 2690–2695, https://doi.org/10.1021/nl061576a.
[29] H. Habib, I.S. Wani, S. Husain, High performance nanostructured symmetric reduced graphene oxide/polyaniline supercapacitor electrode: Effect of polyaniline morphology, J. Energy Storage 55 (2022) 105732, https://doi.org/10.1016/j.est.2022.105732.
[30] X. Jiang, X. Chu, X. Zhang, Y. Xie, T. Yang, J. Huang, W. Li, W. Deng, H. Zhang, W. Yang, Surplus charge injection enables high-cell-potential stable 2D polyaniline supercapacitors, Electrochim. Acta 445 (2023) 142052, https://doi.org/10.1016/j.electacta.2023.142052.
[31] H. Huang, S.C. Abbas, Q. Deng, Y. Ni, S. Cao, X. Ma, An all-paper, scalable and flexible supercapacitor based on vertically aligned polyaniline (PANI) nano-dendrites@fibers, J. Power Sources 498 (2021) 229886, https://doi.org/10.1016/j.jpowsour.2021.229886.
[32] X. Wang, D. Zhang, H. Zhang, L. Gong, Y. Yang, W. Zhao, S. Yu, Y. Yin, D. Sun, In situ polymerized polyaniline/MXene (V2C) as building blocks of supercapacitor and ammonia sensor self-powered by electromagnetic-triboelectric hybrid generator, Nano Energy 88 (2021) 106242, https://doi.org/10.1016/j.nanoen.2021.106242.